A Compact Dual-Band Patch Antenna Design Based on Single-Ring Split Ring Resonator

Ming-Chun Tang [1,2], Hao Wang [1], Li Guo [1], Xiaoping Zeng [1], Hong Liu [2], and Youbing Pang [2]

[1] College of Communication Engineering
Chongqing University, Chongqing 400044, China
tangmingchun@cqu.edu.cn, wangh_2014@126.com, guoli_31@163.com, zxp@cqu.edu.cn

[2] No. 24 Research Institute
China Electronics Technology Group Corporation, Chongqing 400060, China
liuh1981@126.com, pangyb555@163.com

Abstract **–** A compact dual-band patch antenna based on split ring resonator (SRR) element is demonstrated in this paper. In the design, a single-ring SRR, acting as a near-field resonant parasitic (NFRP) element, is integrated in the same plane of radiating patch. The addition of SRR could create a new operational frequency band much lower than the patch fundamental mode, lower the patch resonance frequency, and improve the patch impedance bandwidth significantly, while maintaining the antenna simplicity and compactness. The experimental results are in agreement with the simulation values, demonstrating that our proposed antenna possesses an excellent dual-band radiation performance characteristic, which includes relatively high radiation efficiencies, low cross-polarization levels, and stable broadside radiation performances.

Index Terms **–** Bandwidth improvement, compact patch antenna, dual-band, near-field resonant parasitic element, split ring resonator.

I. INTRODUCTION

Over the past decades, as the common unit cells in metamaterial designs, the split ring resonators (SRRs) and complementary split ring resonators (CSRRs) have attracted much attention because of their interesting resonance response performance characteristics [1-5]. Integration of SRRs and CSRRs in patch antenna design is one of the popular applications in microwave devices, which are comprehensively under investigation in recent years [6-11]. Up to now, there are many successful attempts reported. For example, the stacked SRRs has been utilized to realize the artificial magnetic substrate of patch antenna, which could improve the impedance bandwidth, as well as maintain high radiation efficiency [6]; a double-SRR element was utilized to place at the upper layer of a traditional patch antenna to explore a new and lower resonance frequency [7]; one or two CSRR units were embedded within the radiation patch to achieve dual-band or circularly polarized (CP) operations [8, 9]; and different kinds of CSRRs were placed horizontally between the radiating patch and the ground plane to achieve antenna miniaturization [10]. We also have considered etching CSRRs on the ground around the patch antenna to lower its operational frequency [11].

While effective, above technologies witnessed a certain drawback, which limited their widespread engineering application, arranging SRR above the radiating patch, periodical SRRs within the substrate, or CSRR below the radiating patch may make the design and fabrication quite complicated [6, 7, 10]; etching CSRR slot in the radiating patch may lead to low overall efficiency [8, 9]; and integrating CSRR on the antenna ground may increase the feedline structure impact on radiation patterns [11].

In this paper, a compact dual-band patch antenna based on SRR element is introduced. In the design, a single-ring SRR is loaded in the near field of radiating patch at the same plane to obtain a new and much lower resonance mode, without degradation of the antenna simplicity and compactness. Moreover, the 3rd resonant mode of SRR is located in the vicinity of the patch fundamental mode, which makes the operational bandwidth from the radiation patch witness 18.7% improvement. The prototype of antenna was fabricated and tested. The experimental results, in good agreement with the simulation ones, demonstrate that it exhibits excellent dual-band radiation performances, which include relatively high radiation efficiencies and stable broadside radiation performance within the dual operational bands.

II. ANTENNA DESIGN

Figure 1 gives the geometrical layout of the proposed antenna. As illustrated, a circular radiating patch with the radius R is etched on the top side of a 0.127 mm-thick

Submitted On: June 29, 2015
Accepted On: February 26, 2016

Rogers Duroid 5880 substrate. The value of patch radius (R) is determined by the patch antenna fundamental resonance frequency center, since it is actually a half-wavelength resonator [12]. In details, the thickness of copper film is 0.017 mm and the substrate has the relative permittivity ε_r = 2.2 and loss tangent tan σ = 0.0009. A single-ring SRR, acting as a near-field resonance parasitic (NFRP) element [13, 14], is constructed to surround the patch in the same plane. The center of the SRR is offset away from the patch (L1) to optimize the capacitive coupling between them. The methodology to determine the SRR size will be illustrated in Section IV in details. And a copper ground with the thickness 0.5 mm is placed right under the substrate. The antenna is fed by a coaxial cable with characteristic impedance 50 Ω. The inner probe and outer metallic part of the coax feedline are, respectively, connected with the patch (via the substrate) and the ground. As is shown in Fig. 1 (b), the gap center of SRR, the feeding point, and the centers of patch and SRR are offset with each other but all along with the *x*-axis.

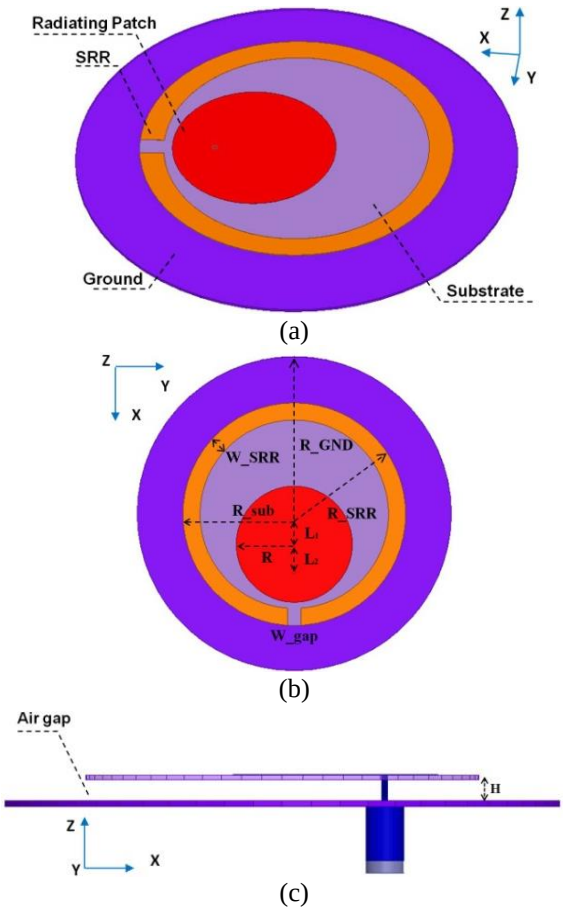

Fig. 1. The configuration of the proposed antenna: (a) 3D view, (b) top view, and (c) side view. Its design parameters are as follows (in millimetre): R_sub = 32.62, R_GND = 46, R_SRR = 32.62, W_gap = 4, W_SRR = 5, R = 16.8, L1 = 8.8, L2 = 7.87, H = 3, and L = 40.

III. ANTENNA PERFORMANCE

The proposed antenna was first simulated with the ANSYS/ANSOFT high frequency structure simulator, HFSS, and then fabricated and tested [15]. The fabricated prototype is shown in Fig. 2. It is noted that, since the substrate is thin and suspended above the ground in the fabricated antenna, several cylindrical rigid foam pillars are placed under the substrate for mechanic supporting in the experimental process.

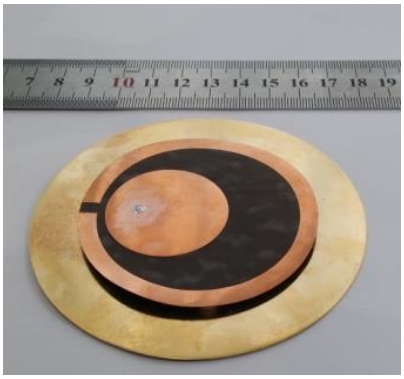

Fig. 2. The fabricated prototype of the proposed antenna.

On one hand, the reflection coefficient of the antenna was measured using Agilent E8361A PNA Vector Network Analyzer (VNA). The measured results together with the corresponding simulation values are plotted in Fig. 3. The experimental (simulation) results indicate that the antenna could provide dual-frequency impedance matching bandwidths with $|S_{11}| < -10$ dB. At lower frequency point 1.602 GHz (1.576 GHz), it has a high impedance matching level with $|S_{11}|_{min}$ = -16.81 dB (-24.16 dB) and a bandwidth 25 MHz (40 MHz), i.e., 1.6% (2.5%) fractional bandwidth. Obviously, the experimental operational frequency center demonstrated 26 MHz blue shift from the simulated one. This acceptable difference (only 1.65%) is quite reasonable, and could be alleviated, if desired, with a careful retuning of the design parameters in Fig. 1. The similar phenomenon was reported in our previous electrically small antenna experimental study [11]. In the higher frequency range, there are two $|S_{11}|$ dips, which are located at 4.5375 GHz (4.550 GHz) and 4.7125 GHz (4.730 GHz), to combine a wide bandwidth 365 MHz (410 MHz), i.e., 8.0% (8.9%) fractional bandwidth. These differences due to the unavoidable errors in the fabrication, installation and measurement process, are deemed to be acceptable. Moreover, in order to emphasize the SRR contributions, the antenna without SRR was simulated as a reference. The simulation results are also shown in Fig. 3 for easy comparison. Note that, all of its constructive parameters are the same as that in Fig. 1. It is observed that, the antenna is also impedance matched to 50 Ω source in the center of 4.600 GHz, with

$|S_{11}|_{min}$ = -21.47 dB. Its -10 dB impedance bandwidth is 347.5 MHz (7.5% fractional bandwidth). By comparison between the simulation results in Fig. 3, it could be easily concluded that, the addition of SRR could create a new much lower operational band, lower the patch resonance frequency center a little, and expand the bandwidth from the patch as high as 18.7% by means of the 3rd resonance mode of SRR, without significant influence on its original impedance match level of the fundamental mode from the patch.

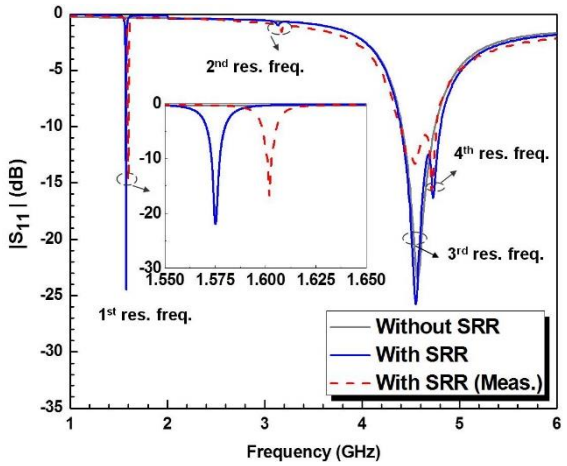

Fig. 3. The simulated and measured reflection coefficients (i.e., $|S_{11}|$ values in dB) for the antennas with and without SRR element.

On the other hand, the far-field radiation patterns of the proposed antenna were measured in an anechoic chamber, which is mainly based on the Agilent EB362C PNA VNA and SATIMO passive measurement system. The measured results together with the corresponding simulation values are shown in Fig. 4. As is shown in Fig. 4 (a), the broadside realized gain is 5.35 dBi in the simulation and 4.59 dBi in the experiment at lower resonance frequency center. And its simulated radiation efficiency is 77.61%. Figures 4 (b) and 4 (c) give the normalized radiation patterns in the upper frequency band. At the two resonance dips of the upper band, the broadside realized gains are 9.91 dBi and 8.58 dBi in the simulation, and 9.48 dBi and 8.17 dBi in the experiment, respectively. Similar to the reported results in Fig. 3, the observed differences between the simulation and experimental results in Fig. 4, while small, arise mainly from the unavoidable errors in the fabrication and measurement process. And its simulated radiation efficiency is higher than 95% over the entire upper band. Moreover, it is easily observed in both simulation and experimental results of Fig. 4, the cross-polarization values in broadside direction are more than 20 dB lower than the co-polarization ones at the three resonance frequency centers, indicating very high linear polarization purity of our proposed antenna. Generally, the broadside radiation performance of antenna is stable.

It should be noted that, lower than -15 dB cross-polarization levels were simultaneously observed in both operational frequency ranges, because of the antenna symmetrical configuration (e.g., ground, patch, and SRR element) along the *x*-axis, resulting in symmetrical current distributions, which will be explained in details in next the section. In addition, because the simulation cross-polarization in the E-plane is lower than −50 dB at each of these frequency points, it was not plotted. In addition, in order to emphasize the design advantages of our proposed antenna clearly, Table 1 is presented for easy comparison between traditional patch antenna and our proposed antenna.

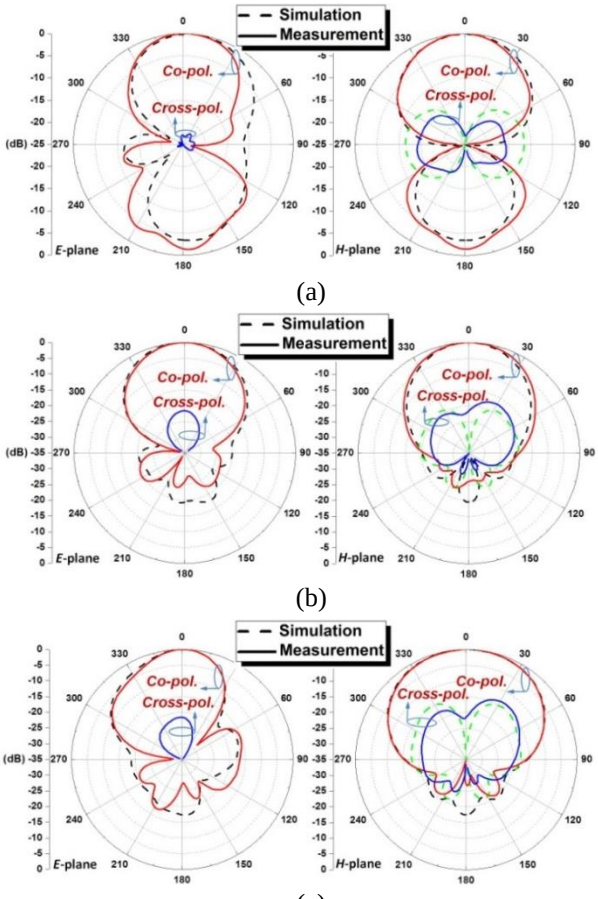

Fig. 4. The simulated and measured normalized radiation patterns at different frequencies in the ZOX plane (*E*-plane) and ZOY plane (*H*-plane): (a) at resonance frequency center of the lower band (1.576 GHz in the simulation and 1.602 GHz in the experiment), (b) at the lower resonance dip of the upper band (4.550 GHz in the simulation and 4.5375 GHz in the experiment), and (c) at the upper resonance dip of the upper band (4.730 GHz in the simulation and 4.7125 GHz in the experiment).

Table 1: Comparisons between traditional patch antenna and our proposed antenna

Category	Traditional Antenna	Proposed Antenna (Sim.)	Proposed Antenna (Exp.)
Lower freq. cent. (GHz)		1.576	1.602
BW in lower freq. range (MHz)		40	25
Gain at lower freq. cent. (dBi)		5.35	4.59
Higher freq. cent. (GHz)	4.600	4.550 & 4.730	4.5375 & 4.7125
BW in higher freq. range (MHz)	347.5	410	365
Gain at higher freq. cent. (dBi)	10.01	9.91 & 8.58	9.48 & 8.17

IV. DISCUSSION

The simulated current distributions on the SRR element and radiating patch at different resonance frequencies are shown in Fig. 5. At the resonance frequency center 1.576 GHz of the lower band, it is observed in Fig. 5 (a) that the majority current is symmetrically concentrated along the SRR surface, which demonstrates that this frequency band is created by SRR electrical resonance [16]. From our calculation, the average electrical length of the current pathway corresponding to 1.576 GHz is l = 92.625 mm = 0.49 λ_{res}, which is very close to half wavelength [16], where,

$$l=(\text{R\_SRR-W\_SRR/2})\times\pi-\text{W\_gap/2}. \quad (1)$$

And then, in Fig. 5 (b), at the 2nd resonance frequency point, i.e., a weak resonance dip around 3.14 GHz in Fig. 3, it is clear that there are two symmetrical anti-phase current pathways along the SRR surface. As is well known, the anti-phase current distribution would lead to a deep null appearance in the radiation pattern in the broadside, which would accordingly degrade the uniformity of the radiation patterns [17]. Thus, the impedance was not optimized to accommodate to 50 Ω source here ($|S_{11}|_{min}$ ~ -1.01 dB). It was worth mentioning that, since its electrical length is twice than the fundamental mode, it could be easily concluded that the SRR resonates in the 2nd harmonic mode at this frequency.

Thirdly, as is shown in Fig. 5 (c), most of the current is polarized on the surface of the radiating patch. Actually, at this frequency point the antenna is operating in TM10 mode. Since a small portion of current is distributed on the SRR, which indicates the SRR has a certain capacitive coupling effect on the patch. Therefore, this resonance frequency center (4.550 GHz) is a little lower than that without SRR (4.600 GHz).

Finally, since the current pathway is three times than that of SRR fundamental mode, it is in theory that the SRR resonates in 3rd harmonic mode, and this phenomenon is confirmed by the current distribution in Fig. 5 (d). Although the antenna at this frequency could exhibit comparable radiation efficiency values to that from the patch resonance in Fig. 5 (c), it is seen that it has a wider beamwidth in H-plane and a little lower broadside realized gain value shown in Fig. 4. The reason is that, at above two different frequency points the antenna operation mechanisms are quite different.

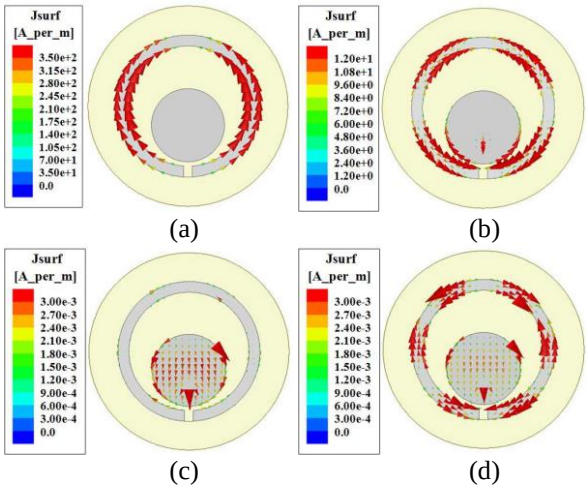

Fig. 5. Simulated current distributions on the radiating patch and SRR element at different resonance frequencies: (a) at resonance frequency center of the lower band (1.576 GHz), (b) at the resonance frequency of 3.14 GHz, (c) at the lower resonance dip of the upper band (4.550 GHz), and (d) at the upper resonance dip of the upper band (4.730 GHz).

In order to comprehensively study our proposed antenna design, two important constructive parameters impact on the antenna impedance performance characteristics is parametrically investigated. Note that, only one parameter is changed and the others remain the same. First, by increasing the SRR gap size (W_gap), it is seen that the first and third modes of SRR shift higher by steps while the fundamental mode of radiating patch almost remains unchanged on the whole, as is shown in Fig. 6 (a). We noted that the resonance frequency of SRR is determined by the formula $f = c/[2l\times(\varepsilon_{eff})^{1/2}]$, where l is average electrical length of the current pathway and is determined by the Equation (1), and $\varepsilon_{eff} \sim (\varepsilon_r+1)/2$ indicates the equivalent relative permittivity. Therefore, when the gap size (W_gap) increases, the total length l decreases, and f goes higher accordingly. Second, the feedline point position effect on the antenna performance is discussed. By changing the position (L2) the SRR fundamental resonance mode is not impacted on the whole, but the 3rd resonance mode of SRR and fundamental resonance mode of the patch are both

affected significantly. Thus, in our optimization process, the impedance matching and impedance bandwidth in the higher frequency band could be improved by only changing the feed position without influence on its performance characteristics in the lower band.

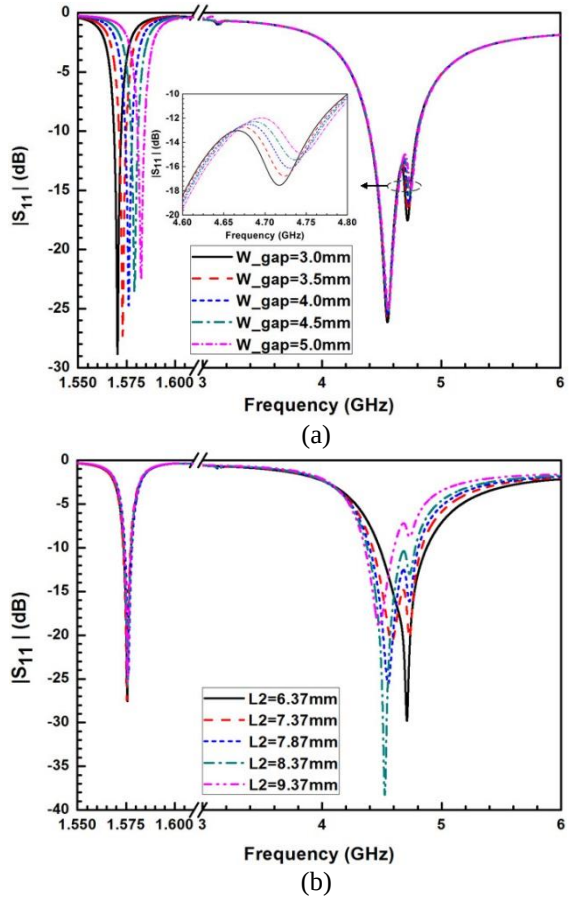

Fig. 6. Impact of two constructive parameters on the antenna impedance matching: (a) the SRR gap size (W_gap), and (b) the feedline point position (L2).

V. CONCLUSION

We proposed a compact, SRR-based, dual-band, NFRP patch antenna. Benefitting from the electrical resonance from SRR element in the near field of radiating patch, a new operational frequency band much lower than the patch fundamental mode is produced, and the fundamental resonance frequency bandwidth of the patch is improved. The addition of SRR has not degraded the antenna simplicity and compactness on the whole. The experimental results, in a good agreement with the simulations, showed that the proposed antenna has high radiation efficiency and stable broadside radiation performances in the two operational bands. Benefiting from its excellent performance characteristic, the proposed compact antenna would be a good candidate in many engineering applications, such as GPS (due to its high polarization purity) [18, 19] and implantable devices (due to its dual-band operation with large dual-frequency interval) [20].

ACKNOWLEDGMENT

This work was supported in part by the National Natural Science Foundation of China contract numbers 61471072 and 91438104, in part by the Focus Project of Chongqing for application and development contract number cstc2013yykfB40009, and in part by the Fundamental Research Funds for the Central Universities contract number 106112015CDJZR165510.

REFERENCES

[1] J. D. Baena, J. Bonache, F. Martin, R. M. Sillero, F. Falcone, T. Lopetegi, M. A. G. Laso, J. Garcia-Garcia, I. Gil, M. F. Portillo, and M. Sorolla, "Equivalent-circuit models for split-ring resonators and complementary split-ring resonators coupled to planar transmission lines," *IEEE Trans. Microw. Theory Tech.*, vol. 53, pp. 1451-1461, 2005.

[2] J. C. Liu, W. Shao, and B. Wang, "A dual-band metamaterial design using double SRR structures," *Appl. Comp. Electro. Society (ACES) Journal*, vol. 26, pp. 459-463, June 2011.

[3] N. Engheta and R. W. Ziolkowski, *Electromagnetic Metamaterials: Physics and Engineering Explorations*, New York, Wiley-IEEE Press, 2006.

[4] D. Jiang, Y. Xu, and R. Xu, "A microstrip printed band-notched UWB antenna using modified CSRR structure," *Appl. Comp. Electro. Society (ACES) Journal*, vol. 28, pp. 521-527, June 2013.

[5] Q. Xiang, Q. Feng, and X. Huang, "Tunable bandstop filter based on split ring resonators loaded Coplanar waveguide," *Appl. Comp. Electro. Society (ACES) Journal*, vol. 28, pp. 591-596, July 2013.

[6] M. Kärkkäinen and P. Ikonen, "Patch antenna with stacked split-ring resonators as an artificial magneto-dielectric substrate," *Microw. Opt. Tech. Lett.*, vol. 46, pp. 554-556, 2005.

[7] O. Quevedo-Teruel, M. N. M. Kehn, and E. Rajo-Iglesias, "Dual-band patch antennas based on short-circuited split ring resonators," *IEEE Trans. Antennas Propag.*, vol. 59, pp. 2758-2765, 2011.

[8] H. Zhang, Y. Q. Li, X. Chen, Y. Q. Fu, and N. C. Yuan, "Design of circular/dual-frequency linear polarization antennas based on the anisotropic complementary split ring resonator," *IEEE Trans. Antennas Propag.*, vol. 57, pp. 3352-3355, 2009.

[9] Y. Dong, H. Toyao, and T. Itoh, "Design and characterization of miniaturized patch antennas loaded with complementary split-ring resonators," *IEEE Trans. Antennas Propag.*, vol. 60, pp. 772-785, 2012.

[10] R. O. Ouedraogo, E. J. Rothwell, A. R. Diaz, K. Fuchi, and A. Temme, "Miniaturization of patch

antennas using a metamaterial-inspired technique," *IEEE Trans. Antennas Propag.*, vol. 60, pp. 2175-2182, 2012.

[11] M.-C. Tang and R. W. Ziolkowski, "A study of low-profile, broadside radiation, efficient, electrically small antennas based on complementary split ring resonators," *IEEE Trans. Antennas Propag.*, vol. 61, pp. 4419-4430, 2013.

[12] I. J. Bhal and P. Bhartia, *Microstrip Antenna*, Dedham, MA: Artech House, 1980.

[13] R. W. Ziolkowski, P. Jin, and C.-C. Lin, "Metamaterial-inspired engineering of antennas," *Proc. IEEE*, vol. 99, pp. 1720-1731, 2011.

[14] M.-C. Tang, R. W. Ziolkowski, S. Xiao, and M. Li, "A high-directivity, wideband, efficient, electrically small antenna system," *IEEE Trans. Antennas Propag.*, vol. 62, pp. 6541-6547, 2014.

[15] ANSYS/ANSOFT High Frequency Structure Simulation (HFSS), ver. 13.0, ANSYS Corp. [Online]. Available at www.ansoft.com.

[16] M.-C. Tang, S. Xiao, D. Wang, J. Xiong, K. Chen, and B. Wang, "Negative index of reflection in planar metamaterial composed of single split-ring resonators," *Appl. Comp. Electro. Society (ACES) Journal*, vol. 26, pp. 250-258, Mar. 2011.

[17] C. A. Balanis, *Antenna Theory: Analysis and Design*, 3rd edition, New York, Wiley Interscience, 2005.

[18] N. Amani and A. Jafargholi, "Internal uniplanar antenna for LTE/WWAN/GPS/GLONASS applications in tablet/laptop computers," *IEEE Antennas Wireless Propag. Lett.*, vol. 14, pp. 1654-1657, 2015.

[19] R. Zhang, H.-H. Kim, and H. Kim, "Triple-band ground radiation antenna for GPS, WiFi 2.4 and 5 GHz band applications," *Electron. Lett.*, vol. 51, no. 25, pp. 2082-2084, Dec. 2015.

[20] C. Liu, Y.-X. Guo, and S. Xiao, "Compact dual-band antenna for implantable devices," *IEEE Antennas Wireless Propag. Lett.*, vol. 11, pp. 1508-1511, 2012.